Template-Stripped Smooth Ag Nanohole Arrays with Silica Shells for Surface Plasmon Resonance Biosensing

Hyungsoon Im,[†] Si Hoon Lee,[‡] Nathan J. Wittenberg,[†] Timothy W. Johnson,[†] Nathan C. Lindquist,[†] Prashant Nagpal,[§] David J. Norris,[⊥] and Sang-Hyun Oh[†,‡,*]

[†]Department of Electrical and Computer Engineering and [‡]Department of Biomedical Engineering, University of Minnesota, Twin Cities, Minneapolis, Minnesota 55455, United States, [§]Los Alamos National Laboratory, Los Alamos, New Mexico 87544, United States, and [⊥]Optical Materials Engineering Laboratory, ETH Zürich, Zürich, Switzerland

ABSTRACT Inexpensive, reproducible, and high-throughput fabrication of nanometric apertures in metallic films can benefit many applications in plasmonics, sensing, spectroscopy, lithography, and imaging. Here we use template-stripping to pattern periodic nanohole arrays in optically thick, smooth Ag films with a silicon template made *via* nanoimprint lithography. Ag is a low-cost material with good optical properties, but it suffers from poor chemical stability and biocompatibility. However, a thin silica shell encapsulating our template-stripped Ag nanoholes facilitates biosensing applications by protecting the Ag from oxidation as well as providing a robust surface that can be readily modified with a variety of biomolecules using well-established silane chemistry. The thickness of the conformal silica shell can be precisely tuned by atomic layer deposition, and a 15 nm thick silica shell can effectively prevent fluorophore quenching. The Ag nanohole arrays with silica shells can also be bonded to polydimethylsiloxane (PDMS) microfluidic channels for fluorescence imaging, formation of supported lipid bilayers, and real-time, label-free SPR sensing. Additionally, the smooth surfaces of the template-stripped Ag films enhance refractive index sensitivity compared with as-deposited, rough Ag films. Because nearly centimeter-sized nanohole arrays can be produced inexpensively without using any additional lithography, etching, or lift-off, this method can facilitate widespread applications of metallic nanohole arrays for plasmonics and biosensing.

KEYWORDS: template-stripping · plasmonics · surface plasmon resonance · nanohole array · atomic layer deposition · microfluidics · biosensing · nanoimprint lithography · supported lipid bilayer

Following the discovery of extraordinary optical transmission (EOT) by Ebbesen *et al.*,[1] metallic films perforated with subwavelength nanoholes have been the focus of intense research in the growing field of plasmonics. These nanostructured films convert incident light into surface plasmons (SPs), which are electromagnetic surface waves that propagate at the metal–dielectric interface. The excitation of SPs modulates the optical transmission spectrum through the nanohole array, generating intense transmission peaks at the wavelengths determined by the shape and periodicity of the nanoholes.[2] Because the spectral resonances can be easily tuned by changing the geometry of the nanostructured film, many potential applications have been proposed, including label-free optical biosensing,[3−13] surface-enhanced spectroscopy,[14−18] and plasmonic photovoltaics.[19−21] Among these applications, label-free kinetic biosensing, in particular, has been widely explored due to the commercial success of surface plasmon resonance (SPR) instruments in pharmaceutical research.[22,23] The existence of commercial SPR instruments such as BIAcore invites the development of more advanced SPR biosensors. However, any novel platform needs to justify the extra design and nanofabrication effort involved either by significantly improving the sensitivity or by enabling new functionality. In this regard, nanohole biosensors have shown many unique capabilities. The platform is based on a simple, low-cost, collinear transmission optical setup, with straightforward alignment allowing the use of high-numerical-aperture imaging optics.[3,10,24] In one example, Lindquist *et al.* showed that a sub-1 μm^2 footprint array can be used for SPR imaging in a dense microarray format.[25] In addition, the unique geometry of metallic nanoholes facilitates the integration of supported lipid bilayer (SLB) membranes[5] or pore-spanning lipid membranes[11] to mimic biochemical reactions occurring on natural cellular membranes. In other work, nanoholes have been used as nanofluidic elements to monitor molecular transport.[26]

Despite these promising applications, costly fabrication of the nanohole sensor chips has been a bottleneck for their widespread dissemination. The majority of existing work utilizes direct patterning of Au films using focused ion beam (FIB) milling or electron-beam lithography (EBL). These serial writing techniques, however, cannot be used for routine production of large-area nanohole array chips. To address this problem, several groups have employed interference

* Address correspondence to sang@umn.edu.

Received for review March 29, 2011 and accepted July 19, 2011.

Published online July 19, 2011
10.1021/nn202013v

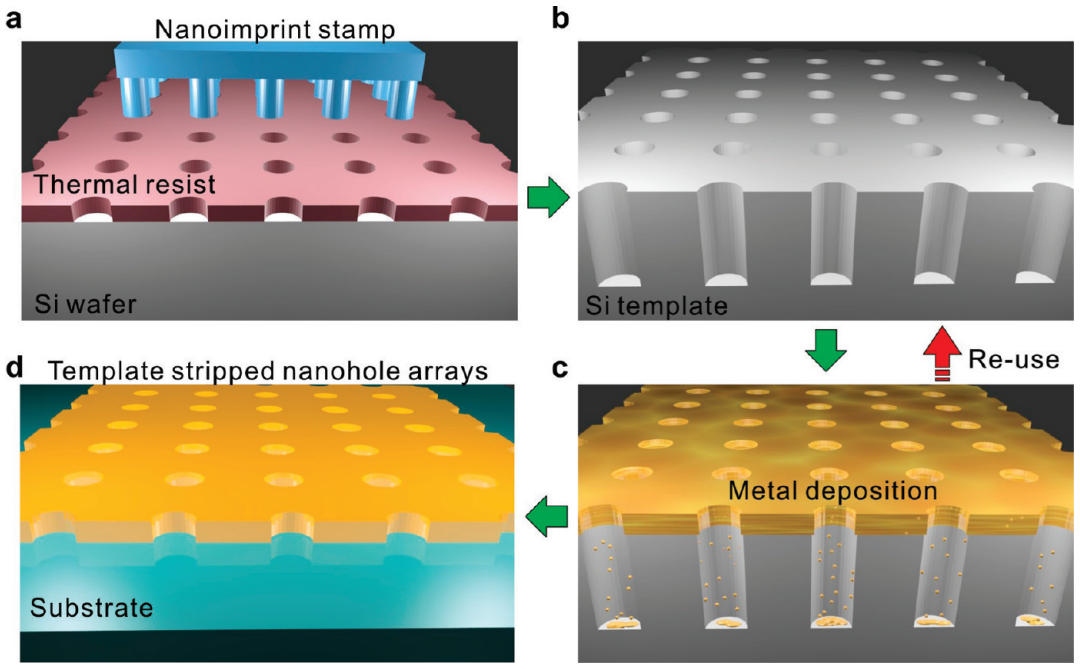

Figure 1. Schematic for fabricating the large-area nanohole arrays. (a) Thermal resist layer spun on a Si wafer is imprinted with a nanoimprint stamp with circular post patterns; (b) Si wafer is subsequently etched to be a nanohole template with deep circular trenches. (c) Metal film is directionally deposited on the Si template. (d) Metal surface is coated with a thin layer of epoxy and covered with a glass slide. The Ag film is then peeled off of the template to reveal the smooth nanohole array made in the metal film. The Si template can be reused to make multiple identical samples.

lithography,[20,24,27,28] nanosphere lithography,[5,16,17] or nanoimprint lithography[6,29,30] to pattern nanoholes over large areas. With conventional interference lithography or nanoimprint lithography, photoresist is spun on the metal film, followed by exposure, development, and patterning by ion milling or lift-off for every chip produced. While nanosphere lithography can eliminate the needs to use a photomask and an exposure system, precise tunability and long-range patterning order cannot be achieved, and in most cases, only optically thin (<50 nm) metal films have been demonstrated. Instead of using direct etching, nanohole arrays can also be fabricated by depositing metals onto a template with deep-hole structures and by removing the perforated metal film, as shown in the advanced soft lithography PEEL technique[27,31] or by a template-stripping method.[32]

The template-stripping technique[32] leverages mature silicon processing technology to make a precisely patterned Si master template. The pattern is then transferred to a deposited metal film, which can be peeled off on demand using an adhesive backing layer. Because a single master template can be repeatedly used to make multiple (>50) copies of the patterned metal films, this process does not require any additional photoresist processing, exposure, etching, or lift-off. Furthermore, the metallic surface obtained by template-stripping retains the smoothness of the crystalline Si master template, typically less than 1−2 nm, in contrast to the rough surfaces of as-deposited metal films.[32] The fabrication of smooth patterned surfaces is essential for applications in plasmonics. Since the electromagnetic fields of SP waves are confined to within 10−100 nm of the metallic surfaces, even nanometric roughness can severely dampen the propagation of SP waves or generate unwanted random "hot spots".[32,33] Previously, template-stripping was used to fabricate nanoholes in optically thin (30 nm) Ag films using a Si template made *via* nanosphere lithography.[32] However, template-stripping of periodic nanoholes in optically thick (>100 nm) metal films remains a challenge. Also, both the Ag nanohole film and the exposed adhesive backing layer should be protected for biosensing in an aqueous environment.

This work combines template-stripping with atomic layer deposition (ALD) to produce periodic nanohole arrays in smooth and optically thick (>100 nm) Ag films, which are subsequently encapsulated with an ALD-grown silica shell for real-time SPR biosensing. Nanoimprint lithography is used to pattern the reusable Si master templates, from which Ag nanohole arrays are replicated with metal deposition and a one-step, peel-off process using optical epoxy as a backing layer. For biosensing, the metallic surface should be modified with molecular recognition elements. Au films are generally preferred for this purpose because they are chemically inert, noncytotoxic, and amenable to well-established surface-modification protocols using self-assembled monolayers.[34] Many groups have also investigated the use of Ag plasmonic structures because they are less expensive than Au while exhibiting lower SP propagation losses in the visible spectrum.[35−37]

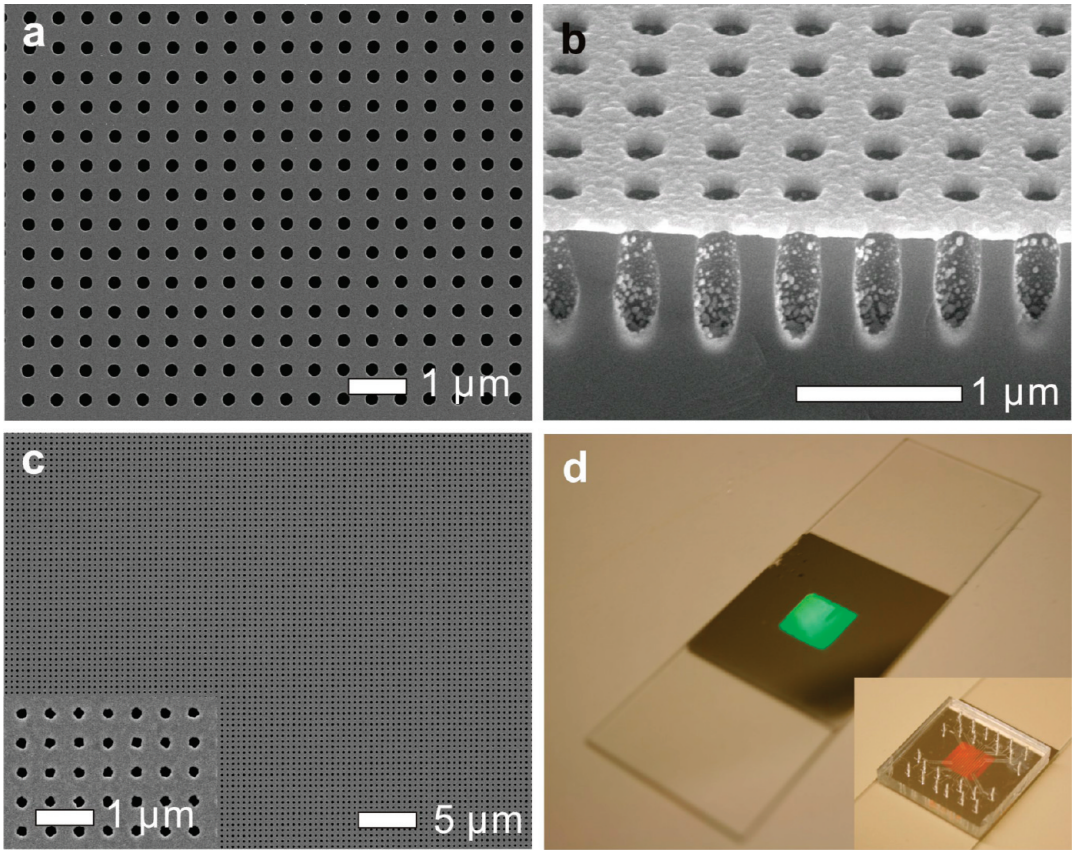

Figure 2. (a) Scanning electron microscope (SEM) image of the Si template with deep circular trenches. (b) Cross-sectional SEM image of the Si template after depositing a 100 nm thick Ag film. (c) SEM image of the template-stripped Ag periodic nanohole array. The inset shows a zoomed-in image of the template-stripped Ag nanoholes. The diameter of the nanoholes and periodicity of the array are 180 and 500 nm, respectively. (d) Photograph of the fabricated nanohole array chip. A 26.5 mm × 26.5 mm area of 100 nm thick Ag film with nanohole patterns in an 8 mm × 8 mm area in the center is transferred to a standard microscope slide. The inset in panel d shows a photograph of a multichannel PDMS chip attached on the silica-coated nanohole array chip.

Working with Ag films, however, presents challenges since they oxidize readily in air or water, and as-deposited Ag films are typically rougher than Au films.[32] Template-stripping can address the challenges of fabricating smooth Ag nanohole arrays with high-throughput. In addition, ALD-grown silica shells play essential roles of protecting both the patterned Ag film and the exposed epoxy substrate while also presenting a uniform surface that is amenable to a wide range of chemical modification techniques. The spectral sensitivity of smooth Ag nanohole arrays is systematically characterized and compared with that of nanohole arrays made in as-deposited Ag films. Formation of self-assembled monolayers and lipid bilayers on the silica-coated nanohole arrays is also demonstrated along with SPR sensing of streptavidin binding to biotinylated lipid bilayers.

RESULTS AND DISCUSSION

Nanohole Array Fabrication *via* Template-Stripping. The template-stripping procedure employed in this paper is illustrated in Figure 1. A Si master template containing a periodic array of deep circular trenches (~600 nm in depth) was first fabricated using nanoimprint lithography followed by deep-trench reactive ion etching. The nanoimprint stamp contains a periodic array of Si posts (210 nm in diameter, 350 nm in height, and 500 nm in periodicity) over an 8 mm × 8 mm area (see Figure S1 in the Supporting Information). After the surface was cleaned, a 100 nm thick Ag film was deposited onto the Si template by e-beam evaporation. Similar to the lift-off process used in standard lithography, here we exploit the poor step coverage to detach Ag atoms deposited in each trench from the Ag film on the top surface of the patterned Si master, as depicted in Figure 1c. Thus a single metal deposition process can create the nanohole patterns in the deposited metal film without using any extra lithography, etching, or ion milling. In this process, it is crucial to reduce the metal deposition on the sidewalls, especially in order to obtain optically thick (>100 nm) Ag films, requiring the formation of vertical sidewalls in the master template and alignment of the metal evaporation source normal to the sample surface. The patterned Ag film was subsequently coated with UV-curable optical epoxy and covered with a glass slide. After the epoxy was cured under UV light, the patterned metallic film, now

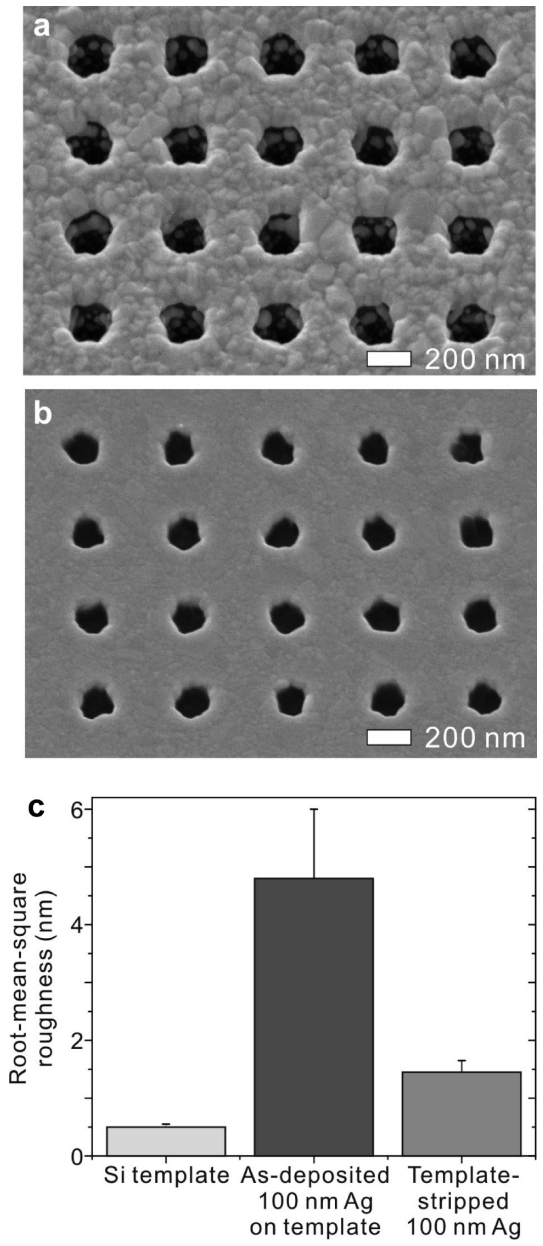

Figure 3. SEM images of (a) an as-deposited 100 nm thick Ag film on the Si template and (b) template-stripped Ag nanoholes peeled off of the template in panel a. (c) Root-mean-square roughness of the Si template (0.5 ± 0.05 nm), the as-deposited 100 nm thick Ag film (4.8 ± 1.2 nm) shown in panel a, and the template-stripped Ag film (1.45 ± 0.2 nm) shown in panel b.

adhered to the glass slide, was peeled off of the template to reveal the smooth buried surface. The Si templates were then cleaned with a 1:1 mixture of sulfuric acid and hydrogen peroxide for 10 min and reused.

Figure 2a shows a top-down scanning electron microscope (SEM) image of a patterned Si template. Figure 2b shows a cross-sectional SEM image of the template after deposition of a 100 nm thick Ag film. The nanohole patterns are created during the single metal evaporation process. Figure 2c shows a SEM image of a template-stripped Ag nanohole array. The hole diameter and periodicity of nanoholes are about 180 and 500 nm, respectively. A photograph of the fabricated nanohole array chip on a glass slide is shown in Figure 2d. The periodic nanohole arrays were made in an 8 mm × 8 mm area centered in a 100 nm thick Ag film with an area of 26.5 mm × 26.5 mm. Alternatively, EBL or FIB can also be used to make the Si templates for making smaller sizes of nanohole arrays (see Figure S2 in the Supporting Information).

The top surfaces of template-stripped Ag nanohole arrays exhibit root-mean-square roughness values below 1−2 nm, while as-deposited 100 nm thick Ag films exhibit roughness of almost 5 nm, as shown in Figure 3.

Optical Characterization of Template-Stripped Ag Nanohole Arrays. The optical transmission spectra of template-stripped Ag nanohole arrays were measured with illumination by a tungsten−halogen lamp through a microscope objective (5×, NA = 0.15) and collected with a fiber-optic spectrometer. Figure 4a shows optical transmission spectra of template-stripped Ag nanohole arrays in contact with different refractive index solutions prepared by mixing water and ethanol, which were injected through a microfluidic cartridge attached to the chip. The transmission spectra were normalized by the spectrum of the incident light source. The measured transmission spectra are uniform across the entire chip area with about 0.1 nm variance in spectral peak positions (data not shown). Figure 4b shows the spectral shift of the transmission minimum around 700 nm as the refractive index of the water−ethanol mixture changes from 1.333 to 1.350, as shown in Figure 4a. The measured bulk refractive index sensitivity is 450 nm/RIU (RIU = refractive index unit). This is about only 10% lower than the theoretical value calculated with finite-difference time-domain (FDTD) simulations (see Figure S3 in the Supporting Information) but higher than previously reported values with similar nanohole dimensions.[3,38]

To examine the spectral sensitivity of Ag nanohole arrays to local changes in the refractive index, thin conformal silica shells were sequentially deposited on the nanohole arrays using ALD. The controlled deposition of a conformal dielectric overlayer on the top and bottom surfaces as well as the sidewalls of the nanohole, analogous to the adsorption of biomolecules, provides a useful method to characterize the sensitivity and dynamic range of SPR biosensors.[37,39] The spectral shifts were measured after depositing sequential 5 nm thick silica shells. For comparison, control samples of nanohole arrays made in evaporated and template-stripped Ag films using FIB were also characterized. Figure 4c shows the spectral shifts of the template-stripped nanohole arrays with the control samples. The sensitivity of the template-stripped nanohole array is similar to the nanohole array made by direct FIB milling in a template-stripped Ag film but about 67% higher than those made with FIB in an as-deposited rough Ag

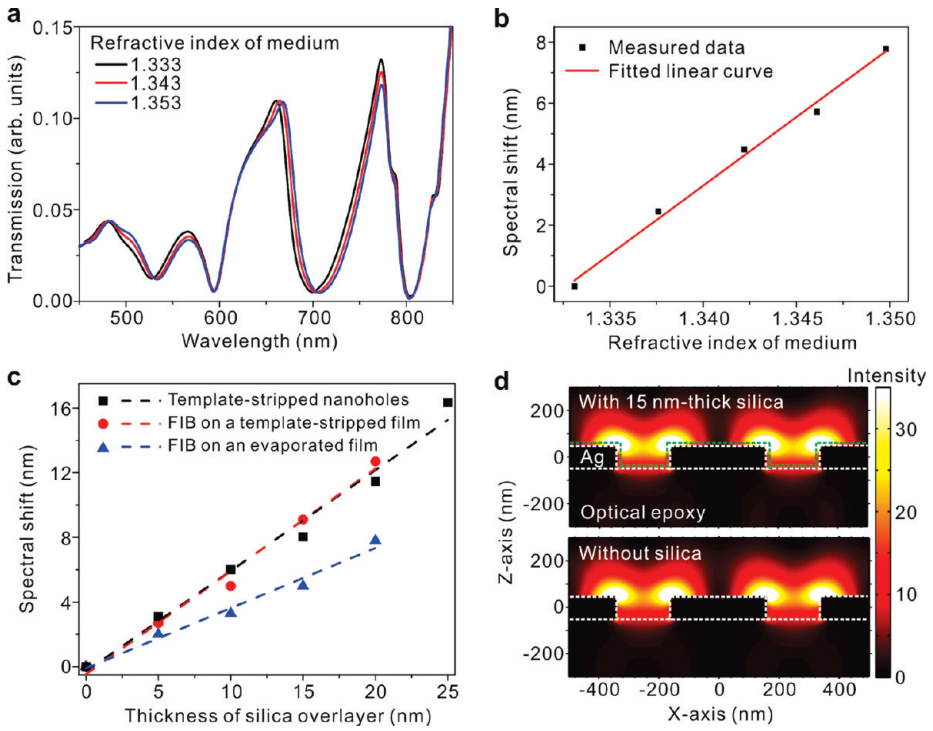

Figure 4. (a) Experimentally measured optical transmission spectra through the nanohole arrays with 180 nm hole size and 500 nm periodicity made in a 100 nm thick Ag film. The bulk refractive index of a water−ethanol mixture on the Ag film varies from 1.333 to 1.350. (b) Bulk refractive index sensitivity measurements of the fabricated nanohole arrays shown in panel a. The spectral shifts are measured as the refractive index of the water−ethanol mixture changes from 1.333 to 1.350. The calculated bulk sensitivity is 450 nm/RIU (RIU = refractive index unit). The solid red line shows a fitted linear curve. (c) Local sensitivity measurements of a template-stripped nanohole array with two control samples made by FIB milling on a template-stripped (smooth) and an evaporated (rough) Ag film. In this case, the spectral shift was measured as the thickness of silica shell deposited *via* ALD increases from 0 to 20 nm. (d) Three-dimensional FDTD simulation of the time-averaged surface plasmon field intensity for template-stripped nanohole arrays with and without a 15 nm thick silica shell.

film. The improved sensitivity can be explained with reduced SP damping due to the smooth surface. Liu *et al.* demonstrated that the sensitivity of a Ag SPR sensor can be enhanced by reducing the roughness of a Ag film deposited with a thin Ni seed layer.[40] Previous work demonstrated that the SP propagation lengths on ultrasmooth template-stripped (sub-1 nm roughness) Ag films increased by a factor of 5−7 in the visible regime compared with standard evaporated Ag films.[32] In a periodic nanohole system, however, the smooth region between adjacent holes is only a few hundred nanometers in size, and SPs also scatter strongly from each nanohole. Thus the effect of smoothness on the EOT spectrum is not as dramatic as the propagation length improvements seen in unpatterned films. Nevertheless, template-stripped Ag nanohole arrays also provide the benefits of high-throughput and low-cost fabrication in addition to the smooth metallic surfaces that improve the overall performance.

ALD Silica Shells and Surface Modification. To avoid unwanted oxidation of Ag surfaces, the template-stripped Ag nanohole arrays were coated by a 15 nm thick silica shell using ALD.[41] Capping the Ag nanohole array with a hydrophilic silica shell not only protects its surface but also enables the use of well-established silane chemistry to covalently attach biomolecules or create a supported or suspended lipid bilayer.[11,42,43] As shown in Figure 4c, the spectral response of the Ag nanohole array remains linear with the deposition of silica shells up to the thickness of ~25 nm, indicating that a 15 nm thick shell still provides sufficient sensitivity. In fact, the refractive index of protein layers and phospholipid bilayers is close to the refractive index of silica,[44,45] making silica shells a useful model for estimating the sensitivity and probing range of nanoplasmonic sensors. To visualize this, Figure 4d shows the simulated distribution of total electric field intensity ($E_x^2 + E_y^2 + E_z^2$) around nanoholes before and after the 15 nm thick silica shell is deposited. It can be seen that the sizes of hot spots, where strong resonant fields are concentrated around the edges of nanoholes, are larger than the thickness of the silica layer and the presence of the shell does not reduce the intensity of the field. The 15 nm thick silica layer is able to protect the Ag nanoholes from harsh oxidizing conditions such as oxygen plasma treatment (see Figure S4 in the Supporting Information). Therefore, it is also possible to permanently bond a polydimethylsiloxane (PDMS) microfluidic chip and silica-coated Ag nanohole arrays without damaging the underlying nanohole arrays. The inset of Figure 2d shows a photograph of a 12-channel microfluidic chip aligned onto the

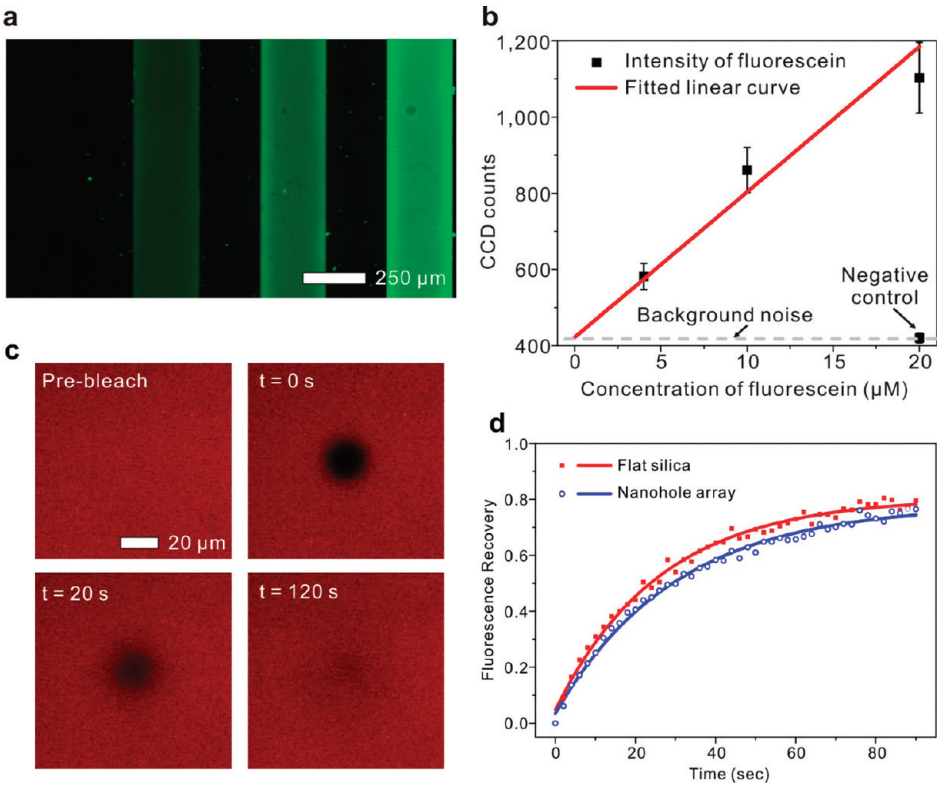

Figure 5. (a) Fluorescence image of template-stripped nanohole arrays covered by a conformal silica layer where the surface is functionalized by a self-assembled monolayer of aminopropyltriethoxysilane (ATPES) in four microfluidic channels with 250 μm width and spacing. The leftmost channel is not functionalized by APTES as a negative control. After the silica surfaces were functionalized, different concentrations of carboxyfluorescein (20, 10, and 4 μM from the rightmost channel) were injected in the presence of EDC. Twenty micromolar carboxyfluorescein without EDC was injected in the leftmost negative control channel. (b) Intensity and linear fit of the carboxyfluorescein fluorescence on each channel surface. The intensity from the negative control is similar to the level of background noise. These indicate that the silica surface is chemically functionalized by APTES and can be used to covalently link different concentrations of molecules in individual microfluidic channels. (c) Frames from a fluorescence recovery after photobleaching (FRAP) experiment on an egg PC supported lipid bilayer with 1% Rhodamine-PE on the silica-coated Ag nanohole array. The time elapsed after photobleaching is indicated in the top left corner. (b) Representative FRAP recovery curves for an egg PC membrane on the silica-coated flat surface (red squares) and a nanohole array (blue circles).

silica-coated nanohole array sample. The inlets and outlets of channels were connected with syringes *via* polytetrafluoroethylene (PTFE) microbore tubes, and syringe pumps were used to control the flow rate of solutions.

To demonstrate surface modification of the template-stripped Ag nanohole arrays with the silica shell, the silica surface was chemically functionalized with aminopropyltriethoxysilane (APTES) solutions to form a self-assembled monolayer (SAM), and fluorophores were then covalently linked to the APTES SAM. Figure 5a shows a fluorescence image of four microfluidic channels where different concentrations of carboxyfluorescein were immobilized on the surface *via* the APTES. The channel width and spacing are 250 μm. In the leftmost channel, phosphate buffered saline (PBS) was injected as a negative control while the other three channels were incubated with 2% (v/v) APTES solutions. After 1 h of incubation, the channels were washed with PBS and 4, 10, and 20 μM of carboxyfluorescein solutions (in the presence of 1-ethyl-3-(3-dimethylaminopropyl)carbodiimide, EDC coupling reagent) were injected for 90 min with a flow rate of 3 μL/min. In the negative control channel, 20 μM of carboxyfluorescein solution was injected without EDC. The fluorescence image was taken after washing the channel with PBS for 10 min with a flow rate of 30 μL/min. Figure 5b shows the fluorescence intensity from each channel shown in Figure 5a. The fluorescence intensity in the negative control channel is similar to the level of background noise, and the fluorescence intensity scales linearly with the concentration of carboxyfluorescein solutions injected. This indicates the silica-coated surface can be chemically functionalized by a SAM of APTES and standard coupling chemistry can be used to attach other molecules. Furthermore, the silica shell prevents quenching by acting as a spacer between the Ag film and the immobilized fluorophores.

In addition to surface modification with APTES, the formation of supported lipid bilayers (SLBs) is demonstrated on the silica surface. SLBs are commonly employed biomimetic structures that allow lipid bilayers to be interfaced with solid-state sensors and microfluidics

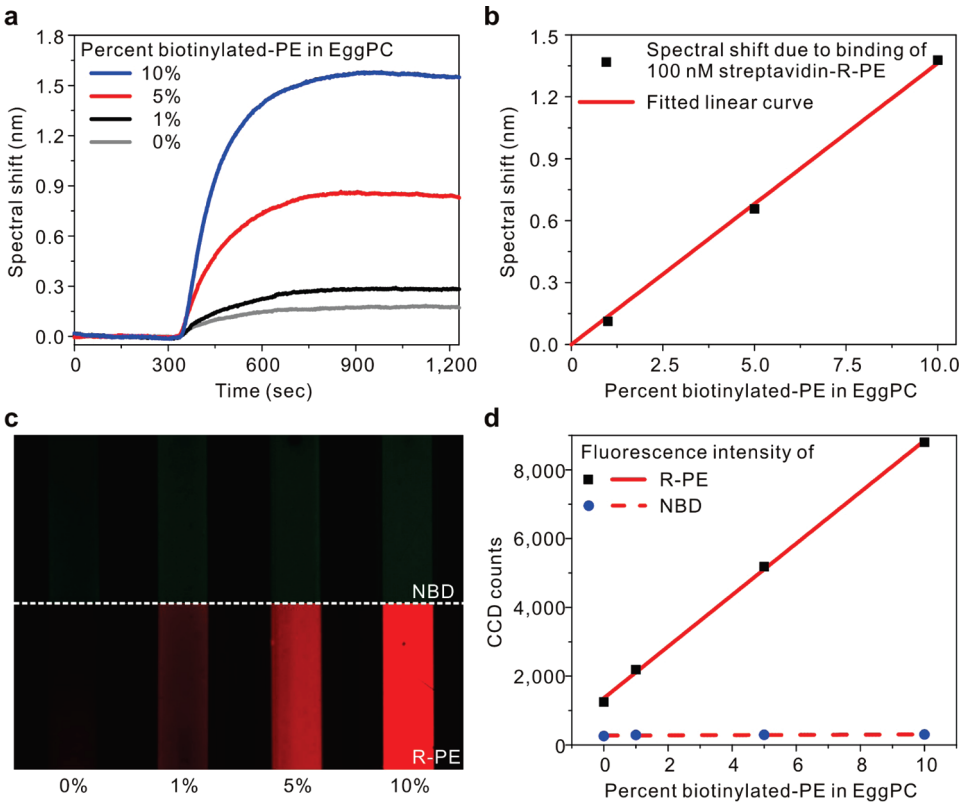

Figure 6. (a) Real-time kinetic measurements of 100 nM of streptavidin-R-phycoerythrin (SAPE) and 1, 5, and 10% biotinylated and nonbiotinylated lipid membranes. After a 5 min baseline with a PBS solution, 100 nM of SAPE in PBS is injected and incubated for 15 min. The flow rate is kept constant at 30 μL/min during SAPE exposure, and data points were recorded every 2 s. (b) Net spectral shift is obtained by subtracting the spectral shift from the binding of SAPE to the nonbiotinylated lipid membrane. This eliminates shifts due to bulk refractive index change and nonspecific binding of SAPE and shifts only from the specific binding of SAPE to biotinylated PE membranes are obtained. The net shifts are fit by a linear curve. (c) Fluorescence images of four channels of nanohole arrays. From the leftmost channel, the percent biotinylated PE in egg PC membrane increases from 0 to 10%. The lipid membranes are tagged by 1% nitrobenzoxadiazole (NBD). Then 100 nM of SAPE is injected through the channels for 15 min. (d) Fluorescence intensity of NBD in the lipid membranes and R-PE after binding with 100 nM SAPE as shown in panel c.

and facilitate incorporation of membrane receptors.[46] The simplest method to form a SLB, and the method used herein, is the spontaneous rupture of vesicles on the hydrophilic silica surface.[47] After allowing Rhodamine-B-labeled vesicles to rupture and form SLBs on silica-coated template-stripped smooth surfaces and nanohole arrays, confocal microscopy and fluorescence recovery after photobleaching (FRAP) were used to characterize the resulting fluorescent SLBs. After thorough washing, the SLBs showed uniform fluorescence on both the flat template-stripped areas, as well as the nanohole arrays (see Figure S5 in the Supporting Information). FRAP confirms that the SLBs formed on both the nanohole array and the flat areas are continuous and allow free planar diffusion of lipids. Figure 5c shows fluorescence images from different time points during a FRAP experiment for a SLB on a template-stripped nanohole array. The nanoholes are not visible in fluorescence mode; however, the presence of nanoholes was confirmed by viewing the sample in transmission mode. After photobleaching, fluorescent lipids diffuse into the bleached area and bleached lipids diffuse outward, resulting in the recovery curves shown in Figure 5d. Notably, the calculated diffusion coefficient (D) is lower for SLBs over nanohole arrays. The diffusion coefficient over the arrays (D_{array}) was calculated to be 1.90 ± 0.15 $\mu m^2/s$, while over flat surfaces, the diffusion coefficient (D_{flat}) was calculated to be 2.25 ± 0.09 $\mu m^2/s$ (mean $\pm$ standard deviation). Using an unpaired t test to compare the means returns a P value of 0.001, indicating that there is a statistically significant difference between the diffusion coefficients. The lower diffusion coefficient over the nanoholes indicates that the membrane probably follows the contours of the nanoporous surface.[48] Brighter fluorescence intensity on a nanohole array area compared with a flat surface also indicates that the SLB conforms to the nanoporous surface. (Detailed analysis is in the Supporting Information.)

Real-Time SPR Biosensing. For SPR biosensing of molecular binding on SLBs, biotinylated SLBs were formed on the silica-coated Ag nanohole array and a solution containing fluorescently labeled streptavidin-R-phycoerythrin (SAPE) was injected into microfluidic channels to

measure binding kinetics of streptavidin to the biotinylated SLBs. The use of fluorescently labeled streptavidin allows simple confirmation of specific binding by fluorescence microscopy. For SLB formation, a PBS solution was injected into the channel with a constant flow rate of 30 μL/min for at least 10 min, and then, a 1 mg/mL of lipid vesicle solution in Tris buffer containing calcium was injected into the channel and incubated for 1 h with a reduced flow rate of 2 μL/h. This was followed by PBS washing for at least 30 min with 50 μL/min to remove excess vesicles. For binding assays, different amounts of biotinylated phosphatidylethanolamine (biotin-PE) were incorporated into egg phosphatidylcholine (egg PC) vesicles and SLBs of the mixtures were formed in each channel by rupture of the vesicles.[49] A biotin-free egg PC membrane was used as a negative control. After 5 min of baseline with a PBS injection, a 100 nM solution of SAPE was injected for 15 min. The flow rate was kept constant at 30 μL/min. Figure 6a shows binding kinetics between 100 nM SAPE and egg PC lipid membranes with 0, 1, 5, and 10% (w/w) biotin-PE as well as 1% (w/w) nitrobenzoxadiazole-conjugated phosphatidylethanolamine (NBD-PE). The EOT spectrum through a Ag nanohole array was recorded every 2 s, and the spectral shift was plotted without any further data processing. The standard deviation of noise (σ) was around 3×10^{-3} nm (shown in Figure S6 in the Supporting Information), and the corresponding resolution (3σ) with the sensitivity of 450 nm/RIU is 2×10^{-5} RIU. The spectral shift shown from the biotin-free egg PC membrane contains a bulk refractive index change and nonspecific binding of SAPE. Therefore, the net shift only due to specific binding of SAPE to biotinylated-PE can be obtained by subtracting the kinetic response between SAPE and the biotin-free egg PC membrane from those between SAPE and biotinylated PE membranes, as shown in Figure 6b. The net shift after subtracting the signal from the negative control channel is linearly proportional to the percent biotinylated PE in the SLB, which indicates that specific binding between SAPE and biotinylated PE can be quantitatively measured from the differential sensing. Figure 6c,d shows fluorescence images and intensities of NBD and SAPE after the kinetic experiments shown in Figure 6a. The fluorescence intensities of NBD conjugated in the lipid membranes from the four channels are all similar regardless of the amount of biotinylated PE, but the intensity of SAPE fluorescence increases linearly as a function of the amount of biotin-PE in the SLB. This confirms that the spectral shifts shown in Figure 6b result from specific binding between SAPE and biotinylated PE membranes.

CONCLUSION

In conclusion, we have produced smooth periodic nanohole arrays over nearly centimeter-sized areas in optically thick Ag films and characterized their optical properties for SPR biosensing applications. By depositing a 15 nm thick silica shell to provide a robust biosensing surface, the Ag film is also protected from unwanted oxidation. A series of experiments including covalent derivatization with APTES, SLB formation, and real-time biosensing with streptavidin and biotinylated lipids demonstrates the utility of low-cost, multifunctional, template-stripped Ag nanohole arrays. Nanoimprint lithography and template-stripping is scalable to high-throughput production because nanoimprint lithography can readily duplicate multiple copies of the reusable Si nanohole templates, all of which can simultaneously and repeatedly produce centimeter-sized nanohole arrays in a single metal evaporation and stripping process. These techniques have the potential to enable broad dissemination of the nanohole-based sensing platform to many researchers who cannot routinely access high-resolution lithography equipment in a cleanroom facility. The improved chemical stability and spectral sensitivity of the smooth Ag nanohole arrays combined with silica shells make this inexpensive platform a promising option for SPR biosensing and plasmonics.

MATERIALS AND METHODS

Fabrication Method. For Si nanohole templates, 4 in. Si wafers were thermally oxidized to grow a 100 nm thick SiO_2 layer. After the Si wafers were spin-coated with thermal imprint resist, NXR-1025 (Nanonex Corp.), and being cured, the Si wafers were imprinted by a Si nanoimprint stamp, which has circular 2D posts with 210 nm diameter, 350 nm depth, and 500 nm periodicity. The SiO_2 and Si were sequentially etched by reactive ion etching (RIE) and deep reactive ion etching (DRIE), respectively, to form about 600 nm deep circular trenches in the Si templates. After the oxide layer was removed by a buffered oxide etchant (BOE), the templates were cleaned by a 1:1 mixture of sulfuric acid and hydrogen peroxide for 5 min. After e-beam evaporation of 100 nm thick Ag film on the Si template, the Ag film was subsequently coated by a UV-curable optical epoxy (NOA 61, Norland Products) and then covered by a glass slide. After the epoxy was cured under UV light, the metallic film perforated with nanoholes, now adhered to the glass slide, was peeled off of the template to reveal the smooth surface. The Si templates were then cleaned by a 1:1 mixture of sulfuric acid and hydrogen peroxide for 10 min and reused to duplicate the nanohole arrays. The detailed fabrication process is described in the Supporting Information.

FDTD Simulation. Full 3D finite-difference time-domain (FDTD) simulations were performed using the commercial software package Fullwave (RSoft Design Group). A unit cell consisting of one hole was used with periodic boundary conditions in two dimensions to simulate an infinite array of periodic nanoholes and perfectly matched layer (PML) boundary conditions were used on the boundaries parallel to the metal surface. The grid used has a constant grid size of 1.5 nm in the plane of the metal and a nominal grid size of 10 nm graded down to 1 nm near the Ag interface in the dimension running through the Ag film. The

complex dielectric constants for the Ag were obtained from Johnson and Christy[50] and numerically fit to a Lorentz-Drude model, and the index of refraction of the epoxy was set to be 1.56. The nanohole arrays were illuminated with a plane wave from the liquid side, and the simulation was run long enough to reach the steady-state solution and the time-averaged total electric field intensity ($E_x^2 + E_y^2 + E_z^2$) was then extracted.

Vesicle Formation. Vesicles were primarily composed of egg PC (L-α-phosphatidylcholine from chicken eggs). For fluorescent vesicles, 1% (w/w) Rhodamine-PE (1,2-dimyristoyl-*sn*-glycero-3-phosphoethanolamine-*N*-lissamine Rhodamine-B sulfonyl, ammonium salt) or 1% NBD-PE (1,2-dimyristoyl-*sn*-glycero-3-phosphoethanolamine-*N*-7-nitro-2-1,3-benzoxadiazol-4-yl, ammonium salt) were included, and for biosensing experiments, various levels of biotin-PE (1,2-dipalmitoyl-*sn*-glycero-3-phosphoethanolamine-*N*-biotinyl, sodium salt) were included (with or without fluorescent lipids) with the egg PC. All lipids were obtained from Avanti Polar Lipids and used without further purification. Vesicles were formed by drying and rehydration followed by extrusion. Lipid solutions in chloroform were dried under vacuum in glass vials for at least 6 h to remove all solvent. Then the dried lipid film was rehydrated with Tris buffer (100 mM NaCl, 10 nM Tris, 1 mM EDTA) and refrigerated overnight. Next the lipids were vortex mixed for 10 s to disperse the vesicles into solution. Extrusion was carried out at room temperature with an Avanti mini-extruder using a polycarbonate membrane with 200 nm holes. Prior to FRAP or biosensing experiments, the vesicles were transferred to Tris buffer containing calcium (100 mM NaCl, 10 mM Tris, 10 mM $CaCl_2$) to facilitate the formation of supported lipid bilayers by vesicle rupture.

FRAP Measurements. For FRAP experiments, SLBs were formed on silica-coated template-stripped substrates by vesicle rupture.[47] The substrates were exposed to vesicle solutions (egg PC/1% (w/w) Rhodamine-PE; 1 mg/mL total lipids) in Tris buffer with calcium for 1 h. After vesicle rupture, the substrates were washed thoroughly with DI water to remove unruptured vesicles and were prevented from drying before and throughout imaging. FRAP was carried out with an Olympus FV1000 upright confocal microscope equipped with a 60× water-immersion objective with a 0.90 numerical aperture. A small circular spot (radius 12−15 μm) on the SLBs was photobleached with simultaneous laser beams at 405, 488, and 543 nm for 10 s. Fluorescence recovery of the photobleached area was monitored by rastering a 543 nm laser spot over the sample and recording an image frame every 2 s. The recovery curves were plotted by determining the average pixel intensity in the bleached area as a function of time using ImageJ software, version 1.44j. Fluorescence intensity was normalized to prebleach values and fit to a single exponential function to determine the time elapsed at which fluorescence had recovered to 50% of the maximum value (t_{50}). The diffusion coefficient (D) for lipids in the SLB was calculated with the following equation: $D = r^2/4t_{50}$, where r is the radius of the photobleached spot.[51,52]

SPR Biosensing Measurements. For kinetic assays in a lipid membrane environment, a 12-channel PDMS microfluidic device with 250 μm wide and 50 μm high channels was assembled on the template-stripped nanohole arrays encapsulated by a 15 nm thick silica layer. Before SLB formation, a PBS solution was injected into the microfluidic channels for at least 10 min to wet the surface. SLB formation was carried out by injecting egg PC vesicles with or without biotin-PE and NBD-PE into the channels with a constant flow rate of 2 μL/h. Only egg PC vesicles without biotin-PE were injected in channels for negative controls. After incubation of vesicles for 1 h to allow vesicle rupture on the silica surface, the channels were washed by PBS for another 30 min with a flow rate of 50 μL/min. After 5 min baseline with the PBS solution, 100 nM of SAPE solution was injected for 15 min, followed by PBS washing for another 15 min. During kinetic assays, the flow rate was kept constant at 30 μL/min by a syringe pump (Harvard Apparatus PHD-2000). The transmission spectra were collected with a microscope objective (50×, NA = 0.55) and fiber-optic spectrometer (Ocean Optics USB4000) and recorded every 2 s. The spectral shifts of the minimum transmission peak around 700 nm were monitored for real-time kinetics of SAPE binding to biotin-PE.

Acknowledgment. This work was supported by grants from the NSF CAREER Award, NSF IDBR Program (DBI-0964216), Office of Naval Research (ONR) Young Investigator Program, and NIH R01 GM 092993 (S.-H.O.). H.I. acknowledges a 3M Science and Technology Fellowship. S.H.L. was supported by a Samsung Fellowship. T.W.J. acknowledges an NIH Biotechnology training grant. Device fabrication was performed at the U. of Minnesota Nanofabrication Center (NFC), which receives support from NSF through the National Nanotechnology Infrastructure Network.

Supporting Information Available: Detailed experimental methods and supporting Figures S1−S6. This material is available free of charge *via* the Internet at http://pubs.acs.org.

REFERENCES AND NOTES

1. Ebbesen, T. W.; Lezec, H. J.; Ghaemi, H. F.; Thio, T.; Wolff, P. A. Extraordinary Optical Transmission through Sub-wavelength Hole Arrays. *Nature* **1998**, *391*, 667–669.
2. Genet, C.; Ebbesen, T. W. Light in Tiny Holes. *Nature* **2007**, *445*, 39–46.
3. Brolo, A. G.; Gordon, R.; Leathem, B.; Kavanagh, K. L. Surface Plasmon Sensor Based on the Enhanced Light Transmission through Arrays of Nanoholes in Gold Films. *Langmuir* **2004**, *20*, 4813–4815.
4. Ramachandran, N.; Larson, D. N.; Stark, P. R. H.; Hainsworth, E.; LaBaer, J. Emerging Tools for Real-Time Label-Free Detection of Interactions on Functional Protein Microarrays. *FEBS J.* **2005**, *272*, 5412–5425.
5. Dahlin, A.; Zäch, M.; Rindzevicius, T.; Käll, M.; Sutherland, D. S.; Höök, F. Localized Surface Plasmon Resonance Sensing of Lipid-Membrane-Mediated Biorecognition Events. *J. Am. Chem. Soc.* **2005**, *127*, 5043–5048.
6. Stewart, M. E.; Mack, N. H.; Malyarchuk, V.; Soares, J.; Lee, T. W.; Gray, S. K.; Nuzzo, R. G.; Rogers, J. A. Quantitative Multispectral Biosensing and 1D Imaging Using Quasi-3D Plasmonic Crystals. *Proc. Natl. Acad. Sci. U.S.A.* **2006**, *103*, 17143–17148.
7. Lesuffleur, A.; Im, H.; Lindquist, N. C.; Oh, S. H. Periodic Nanohole Arrays with Shape-Enhanced Plasmon Resonance as Real-Time Biosensors. *Appl. Phys. Lett.* **2007**, *90*, 243110.
8. Pang, L.; Hwang, G. M.; Slutsky, B.; Fainman, Y. Spectral Sensitivity of Two-Dimensional Nanohole Array Surface Plasmon Polariton Resonance Sensor. *Appl. Phys. Lett.* **2007**, *91*, 123112.
9. Yang, J. C.; Ji, J.; Hogle, J. M.; Larson, D. N. Metallic Nanohole Arrays on Fluoropolymer Substrates as Small Label-Free Real-Time Bioprobes. *Nano Lett.* **2008**, *8*, 2718–2724.
10. Im, H.; Lesuffleur, A.; Lindquist, N. C.; Oh, S. H. Plasmonic Nanoholes in a Multichannel Microarray Format for Parallel Kinetic Assays and Differential Sensing. *Anal. Chem.* **2009**, *81*, 2854–2859.
11. Im, H.; Wittenberg, N. J.; Lesuffleur, A.; Lindquist, N. C.; Oh, S.-H. Membrane Protein Biosensing with Plasmonic Nanopore Arrays and Pore-Spanning Lipid Membranes. *Chem. Sci.* **2010**, *1*, 688–696.
12. Yanik, A. A.; Huang, M.; Kamohara, O.; Artar, A.; Geisbert, T. W.; Connor, J. H.; Altug, H. An Optofluidic Nanoplasmonic Biosensor for Direct Detection of Live Viruses from Biological Media. *Nano Lett.* **2010**, *10*, 4962–4969.
13. Lee, K. L.; Wei, P. K. Enhancing Surface Plasmon Detection Using Ultrasmall Nanoslits and a Multispectral Integration Method. *Small* **2010**, *6*, 1900–1907.
14. Brolo, A. G.; Arctander, E.; Gordon, R.; Leathem, B.; Kavanagh, K. L. Nanohole-Enhanced Raman Scattering. *Nano Lett.* **2004**, *4*, 2015–2018.
15. Coe, J. V.; Heer, J. M.; Teeters-Kennedy, S.; Tian, H.; Rodriguez, K. R. Extraordinary Transmission of Metal Films with Arrays of Subwavelength Holes. *Annu. Rev. Phys. Chem.* **2008**, *59*, 179–202.
16. Lee, S.; Bantz, K.; Lindquist, N.; Oh, S.; Haynes, C. Self-Assembled Plasmonic Nanohole Arrays. *Langmuir* **2009**, *25*, 13685–13693.
17. Masson, J. F.; Murray-Methot, M. P.; Live, L. S. Nanohole Arrays in Chemical Analysis: Manufacturing Methods and Applications. *Analyst* **2010**, *135*, 1483–1489.

18. Im, H.; Bantz, K. C.; Lindquist, N. C.; Haynes, C. L.; Oh, S. H. Vertically Oriented Sub-10-nm Plasmonic Nanogap Arrays. *Nano Lett.* **2010**, *10*, 2231–2236.
19. Ferry, V. E.; Verschuuren, M. A.; Li, H.; Schropp, R. E. I.; Atwater, H. A.; Polman, A. Improved Red-Response in Thin Film a-Si:H Solar Cells with Soft-Imprinted Plasmonic Back Reflectors. *Appl. Phys. Lett.* **2009**, *95*, 183503.
20. Menezes, J. W.; Ferreira, J.; Santos, M. J. L.; Cescato, L.; Brolo, A. G. Large-Area Fabrication of Periodic Arrays of Nanoholes in Metal Films and Their Application in Biosensing and Plasmonic-Enhanced Photovoltaics. *Adv. Funct. Mater.* **2010**, *20*, 3918–3924.
21. Atwater, H. A.; Polman, A. Plasmonics for Improved Photovoltaic Devices. *Nat. Mater.* **2010**, *9*, 205–213.
22. Cooper, M. A. Advances in Membrane Receptor Screening and Analysis. *J. Mol. Recognit.* **2004**, *17*, 286–315.
23. Homola, J. Surface Plasmon Resonance Sensors for Detection of Chemical and Biological Species. *Chem. Rev.* **2008**, *108*, 462–493.
24. Tetz, K. A.; Pang, L.; Fainman, Y. High-Resolution Surface Plasmon Resonance Sensor Based on Linewidth-Optimized Nanohole Array Transmittance. *Opt. Lett.* **2006**, *31*, 1528–1530.
25. Lindquist, N. C.; Lesuffleur, A.; Im, H.; Oh, S. H. Sub-micron Resolution Surface Plasmon Resonance Imaging Enabled by Nanohole Arrays with Surrounding Bragg Mirrors for Enhanced Sensitivity and Isolation. *Lab Chip* **2009**, *9*, 382–387.
26. Eftekhari, F.; Escobedo, C.; Ferreira, J.; Duan, X.; Girotto, E. M.; Brolo, A. G.; Gordon, R.; Sinton, D. Nanoholes as Nanochannels: Flow-Through Plasmonic Sensing. *Anal. Chem.* **2009**, *81*, 4308–4311.
27. Henzie, J.; Lee, M. H.; Odom, T. W. Multiscale Patterning of Plasmonic Metamaterials. *Nat. Nanotechnol.* **2007**, *2*, 549–554.
28. Odom, T. W.; Gao, H. W.; McMahon, J. M.; Henzie, J.; Schatz, G. C. Plasmonic Superlattices: Hierarchical Subwavelength Hole Arrays. *Chem. Phys. Lett.* **2009**, *483*, 187–192.
29. Chen, J.; Shi, J.; Decanini, D.; Cambril, E.; Chen, Y.; Haghiri-Gosnet, A. M. Gold Nanohole Arrays for Biochemical Sensing Fabricated by Soft UV Nanoimprint Lithography. *Microelectron. Eng.* **2009**, *86*, 632–635.
30. Yang, J. C.; Gao, H. W.; Suh, J. Y.; Zhou, W.; Lee, M. H.; Odom, T. W. Enhanced Optical Transmission Mediated by Localized Plasmons in Anisotropic, Three-Dimensional Nanohole Arrays. *Nano Lett.* **2010**, *10*, 3173–3178.
31. Henzie, J.; Lee, J.; Lee, M.; Hasan, W.; Odom, T. Nanofabrication of Plasmonic Structures. *Annu. Rev. Phys. Chem.* **2009**, *60*, 147–165.
32. Nagpal, P.; Lindquist, N. C.; Oh, S. H.; Norris, D. J. Ultrasmooth Patterned Metals for Plasmonics and Metamaterials. *Science* **2009**, *325*, 594–597.
33. Lindquist, N. C.; Nagpal, P.; Lesuffleur, A.; Norris, D. J.; Oh, S. H. Three-Dimensional Plasmonic Nanofocusing. *Nano Lett.* **2010**, *10*, 1369–1373.
34. Love, J. C.; Estroff, L. A.; Kriebel, J. K.; Nuzzo, R. G.; Whitesides, G. M. Self-Assembled Monolayers of Thiolates on Metals as a Form of Nanotechnology. *Chem. Rev.* **2005**, *105*, 1103–1169.
35. Zhang, X. Y.; Zhao, J.; Whitney, A. V.; Elam, J. W.; Van Duyne, R. P. Ultrastable Substrates for Surface-Enhanced Raman Spectroscopy: Al_2O_3 Overlayers Fabricated by Atomic Layer Deposition Yield Improved Anthrax Biomarker Detection. *J. Am. Chem. Soc.* **2006**, *128*, 10304–10309.
36. Gao, H. W.; Henzie, J.; Lee, M. H.; Odom, T. W. Screening Plasmonic Materials Using Pyramidal Gratings. *Proc. Natl. Acad. Sci. U.S.A.* **2008**, *105*, 20146–20151.
37. Im, H.; Lindquist, N. C.; Lesuffleur, A.; Oh, S. H. Atomic Layer Deposition of Dielectric Overlayers for Enhancing the Optical Properties and Chemical Stability of Plasmonic Nanoholes. *ACS Nano* **2010**, *4*, 947–954.
38. Murray-Méthot, M. P.; Ratel, M.; Masson, J. F. Optical Properties of Au, Ag, and Bimetallic Au on Ag Nanohole Arrays. *J. Phys. Chem. C* **2010**, *114*, 8268–8275.
39. Whitney, A. V.; Elam, J. W.; Zou, S. L.; Zinovev, A. V.; Stair, P. C.; Schatz, G. C.; Van Duyne, R. P. Localized Surface Plasmon Resonance Nanosensor: A High-Resolution Distance-Dependence Study Using Atomic Layer Deposition. *J. Phys. Chem. B* **2005**, *109*, 20522–20528.
40. Liu, H.; Wang, B.; Leong, E. S. P.; Yang, P.; Zong, Y.; Si, G. Y.; Teng, J. H.; Maier, S. A. Enhanced Surface Plasmon Resonance on a Smooth Silver Film with a Seed Growth Layer. *ACS Nano* **2010**, *4*, 3139–3146.
41. Hausmann, D.; Becker, J.; Wang, S. L.; Gordon, R. G. Rapid Vapor Deposition of Highly Conformal Silica Nanolaminates. *Science* **2002**, *298*, 402–406.
42. Jonsson, M. P.; Jönsson, P.; Dahlin, A. B.; Höök, F. Supported Lipid Bilayer Formation and Lipid-Membrane-Mediated Biorecognition Reactions Studied with a New Nanoplasmonic Sensor Template. *Nano Lett.* **2007**, *7*, 3462–3468.
43. Guo, P. F.; Wu, S.; Ren, Q. J.; Lu, J.; Chen, Z. H.; Xiao, S. J.; Zhu, Y. Y. Fluorescence Enhancement by Surface Plasmon Polaritons on Metallic Nanohole Arrays. *J. Phys. Chem. Lett.* **2010**, *1*, 315–318.
44. Voros, J. The Density and Refractive Index of Adsorbing Protein Layers. *Biophys. J.* **2004**, *87*, 553–561.
45. Vockenroth, I. K.; Atanasova, P. P.; Jenkins, A. T. A.; Koper, I. Incorporation of α-Hemolysin in Different Tethered Bilayer Lipid Membrane Architectures. *Langmuir* **2008**, *24*, 496–502.
46. Castellana, E. T.; Cremer, P. S. Solid Supported Lipid Bilayers: From Biophysical Studies to Sensor Design. *Surf. Sci. Rep.* **2006**, *61*, 429–444.
47. Brian, A. A.; McConnell, H. M. Allogeneic Stimulation of Cyto-toxic T-Cells by Supported Planar Membranes. *Proc. Natl. Acad. Sci. U.S.A.* **1984**, *81*, 6159–6163.
48. Jönsson, P.; Jonsson, M. P.; Höök, F. Sealing of Submicrometer Wells by a Shear-Driven Lipid Bilayer. *Nano Lett.* **2010**, *10*, 1900–1906.
49. Yang, T. L.; Jung, S. Y.; Mao, H. B.; Cremer, P. S. Fabrication of Phospholipid Bilayer-Coated Microchannels for On-Chip Immunoassays. *Anal. Chem.* **2001**, *73*, 165–169.
50. Johnson, P. B.; Christy, R. W. Optical Constants of the Noble Metals. *Phys. Rev. B* **1972**, *6*, 4370.
51. Axelrod, D.; Koppel, D. E.; Schlessinger, J.; Elson, E.; Webb, W. W. Mobility Measurement by Analysis of Fluorescence Photobleaching Recovery Kinetics. *Biophys. J.* **1976**, *16*, 1055–1069.
52. Soumpasis, D. M. Theoretical-Analysis of Fluorescence Photobleaching Recovery Experiments. *Biophys. J.* **1983**, *41*, 95–97.